Accelerated infected wound healing by probiotic-based living microneedles with long-acting antibacterial effect

Yinli Jin [a,1], Yun Lu [d,1], Xue Jiang [a,1], Min Wang [c], Yaqi Yuan [a], Yongnian Zeng [a], Liang Guo [c,**], Wei Li [a,b,*]

[a] Department of Thyroid and Breast Surgery, Zhongnan Hospital of Wuhan University, School of Pharmaceutical Sciences, Wuhan University, Wuhan, 430071, China
[b] TaiKang Center for Life and Medical Sciences, Wuhan University, Wuhan, China
[c] Department of Plastic Surgery, Zhongnan Hospital of Wuhan University, Wuhan, China
[d] Department of Pharmacy, Zhongnan Hospital of Wuhan University, Wuhan, China

ABSTRACT

Delays in infected wound healing are usually a result of bacterial infection and local inflammation, which imposes a significant and often underappreciated burden on patients and society. Current therapies for chronic wound infection generally suffer from limited drug permeability and frequent drug administration, owing to the existence of a wound biofilm that acts as a barrier restricting the entry of various antibacterial drugs. Here, we report the design of a biocompatible probiotic-based microneedle (MN) patch that can rapidly deliver beneficial bacteria to wound tissues with improved delivery efficiency. The probiotic is capable of continuously producing antimicrobial substances by metabolizing introduced glycerol, thereby facilitating infected wound healing through long-acting antibacterial and anti-inflammatory effects. Additionally, the beneficial bacteria can remain highly viable (>80 %) inside MNs for as long as 60 days at 4 °C. In a mouse model of *Staphylococcus aureus*-infected wounds, a single administration of the MN patch exhibited superior antimicrobial efficiency and wound healing performance in comparison with the control groups, indicating great potential for accelerating infected wound closure. Further development of live probiotic-based MN patches may enable patients to better manage chronically infected wounds.

1. Introduction

Infected wounds are disorders in which the wounds remain infected by bacteria or other microorganisms during the curing process [1]. Common bacteria that can induce wound infections include *Staphylococcus aureus* (*S. aureus*), *Pseudomonas aeruginosa* (*P. aeruginosa*), and *Escherichia coli* (*E. coli*) [2]. Unlike acute wounds, chronically infected wounds generally undergo a prolonged healing process and may not heal completely [3]. Moreover, the incidence of chronically infected wounds is relatively high among susceptible populations, such as bedridden patients [4], diabetics [5], and those with compromised immune systems, which makes them more prone to bacterial infections and causes additional economic and emotional patient burdens [6,7].

Currently, there are various therapeutic methods available for infected wound treatment, including regular wound debridement [8], oral antibiotics [9], antibacterial dressings [10,11], negative pressure wound therapy [12,13], functional hydrogels [14], microparticles [15], and physical approaches like laser treatment [16,17]. Although these approaches have shown some efficacy in wound management, either by inhibiting bacterial growth in the wound or by applying growth factors to accelerate wound healing, their widespread application remains limited by certain drawbacks. First, the biofilm generated by bacteria at the wound site forms a physical barrier that restricts the penetration of antimicrobial agents or biological macromolecules into deep tissues, thereby significantly reducing drug delivery efficiency [18–20]. Second, the misuse and overuse of antibiotics are the main drivers that increase

the risk of antibiotic resistance, which has become a serious global health concern [21]. In addition, frequent dressing changes are usually required, which may cause pain and secondary injury to the wound, thereby significantly reducing patient compliance [22]. Therefore, a new therapeutic strategy for wound healing that is minimally invasive, facilitates drug penetration into wounds, and achieves long-term efficacy is highly desirable.

Recently, the application of probiotics for antibacterial effects in wound tissue has attracted considerable interest because beneficial bacteria are safe and capable of removing deleterious bacteria from wound sites by competing with nutrition or producing antimicrobial substances that are suitable for their survival but harmful to the deleterious bacteria, thereby avoiding frequent administration of antimicrobial agents or eliminating the risk of drug resistance [23]. As one of the most widely used probiotic bacteria, *Lactobacillus reuteri* (*L. reuteri*) mostly exists in the gastrointestinal tract, and has been commonly reported to benefit the host immune system by reducing the production of pro-inflammatory cytokines and promoting regulatory T cell development and function [24,25]. Owing to these features, probiotics such as hydrogel dressings have been developed into formulations to promote infected wound healing [26,27]. To protect the activity of probiotics, various biomaterials have been utilized for probiotic delivery, such as hyaluronic acid-based hydrogels [28], soybean protein-based microparticles [29], and alginate-starch microgels [30,31], which provide good protection against various stress factors during encapsulation, storage, and delivery, including pH, temperature, and oxygen. Although some progress has been made, maintaining high viability of beneficial bacteria and a long-acting antimicrobial effect in deep tissue remains unexplored.

Over the past two decades, microneedles (MNs) that can bypass physical barriers (e.g., the stratum corneum) and directly deliver payloads into deep tissues have emerged as an appealing therapeutic modality for transdermal drug delivery with increased stability and enhanced delivery efficiency [32–34]. Owing to their unique properties, MNs have been widely used in a number of biomedical applications, including contraception [35], diabetes treatment [36], hair regrowth [37], gout management [38], and cancer therapy [39]. Recently, MNs

have also been adopted for the transdermal delivery of live organisms such as probiotics [40]. For instance, in 2018, Chen et al. reported an MN patch for the delivery of live probiotics to the skin for the first time, demonstrating the biosafety of probiotics in local skin without causing any tissue irritation [41]. Recently, Enggi et al. developed another dissolving MN patch integrated with probiotic-loaded multilayer microcapsules to improve the treatment of vulvovaginal candidiasis, with high therapeutic efficiency and satisfactory biosafety [42]. Compared to other formulations for probiotic delivery, such as microparticles and hydrogels [43,44], MNs that enable self-administration, improved delivery efficiency, and avoided hypodermic injection exhibited superior therapeutic efficacy and improved patient compliance with probiotic treatment in a minimally invasive manner. Despite the above achievements, the design of MN patches for transdermal delivery of probiotics to accelerate infected wound healing has not yet been explored, primarily because of the long-term healing process of wounds, which usually requires the long-acting antibacterial effect of probiotics in the wound.

Here, we report an engineered *Lactobacillus reuteri* (*L. reuteri*)-loaded MN patch (termed the 5 % glycerol [GL] MN patch) that promotes infected wound healing. The 5 % GL MN patches were made of polyvinyl alcohol (PVA), sucrose, 5 % glycerol, and the probiotic *L. reuteri* (Fig. 1a). We selected *L. reuteri* as the probiotic model because it is biocompatible, naturally present in the human body, and has been reported to metabolize glycerol to generate a non-proteinaceous broad-spectrum antibacterial substance called reuterin (Fig. 1b) [45–47]. The PVA-sucrose matrix provided sufficient mechanical strength for MNs and facilitated the rapid dissolution of MNs after skin insertion, thereby realizing fast delivery of the probiotic *L.* reuteri to wounds. The deMan Rogosa Sharpe (MRS) medium was added to the polymeric mixture when making the MNs, which aimed to provide nutrients for the loaded beneficial bacteria. The MN patch was dried under a mild condition (i.e., at room temperature) to avoid the damage to the encapsulated *L. reuteri* in the MNs. It is worth noting that the inclusion of glycerol in MNs did not affect the survival of *L. reuteri* but provided the probiotic with an adequate source for continuously producing reuterin, thus achieving long-acting antimicrobial and anti-inflammatory effects in the deep wound (Fig. 1c). Inside MNs, *L. reuteri* could remain highly viable for
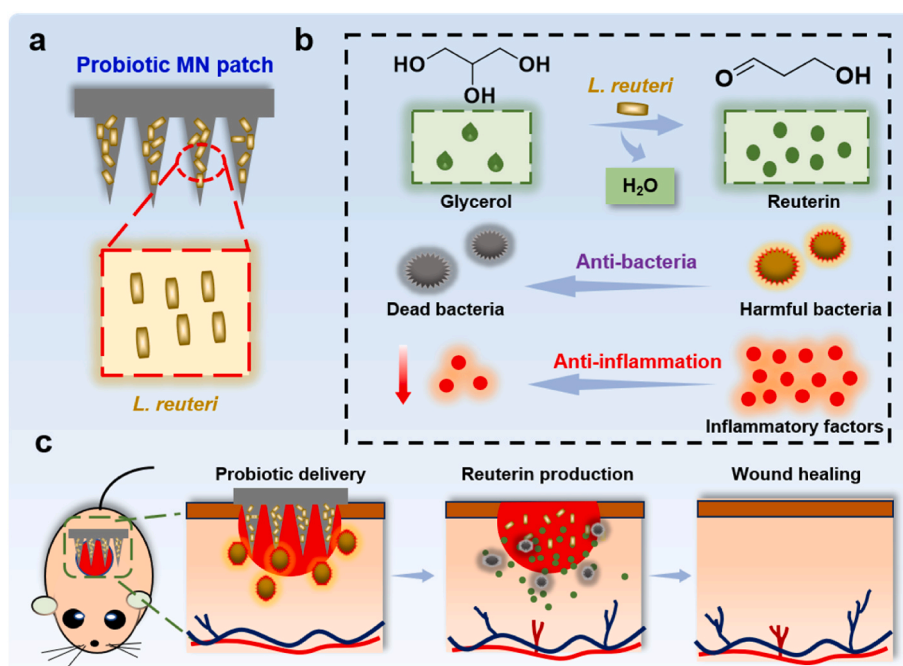

Fig. 1. Schematic of 5 % GL MN patch for chronic infected wound healing. (a) Schematic illustration of 5 % GL MN patch containing the probiotic of *L. reuteri*. (b) Working mechanism of *L. reuteri* with antibacterial and anti-inflammatory effect. (c) Schematic illustration of 5 % GL MN patch with long-acting antimicrobial effect for accelerating infected wound healing.

more than 7 days at room temperature or 60 days at 4 °C. Owing to the above features, a single administration of the 5 % GL MN patch exhibited superior antimicrobial efficacy and accelerated wound healing in a mouse model of *S. aureus*-infected wounds compared to other groups, including the blank MNs group, MNs group without glycerol, and MNs group containing reuterin, indicating the long-term effect of the designed MN patch on eliminating harmful bacteria, reducing inflammation, and promoting wound closure. Therefore, we believe that the live probiotic-based MN patch introduced in this study provides a novel alternative to current management strategies for facilitating infected wound healing.

2. Results

2.1. Fabrication and characterization of MN patches

To investigate the optimal glycerol content in probiotic-loaded MN patches, a vacuum-assisted micromolding method was used to fabricate MN patches containing different glycerol concentrations: 0 %, 2.5 %, 5 %, 10 %, and 15 % (i.e., 0 % GL MNs, 2.5 % GL MNs, 5 % GL MNs, 10 % GL MNs, and 15 % GL MNs) (Fig. 2a and b). Patches with 0 % GL, 2.5 GL, 5 % GL, and 10 % GL MNs, could be successfully prepared with this fabrication method, with intact MNs bound to the patch backings; however, it was difficult to make 15 % GL MNs with an unbroken structure due to the excessive glycerol content, which caused breakage of MNs during the demolding process (Fig. 2b). The fabricated MNs with different glycerol contents were applied to pig skin ex vivo to examine their mechanical strength. For better visualization, the MNs were loaded with the fluorescent dye Rhodamine B. As shown in Fig. 2d, MNs with GL

concentrations ranging from 0 % to 5 % displayed efficient insertion and dissolution capabilities during skin application, showing approximately 100 % penetration efficiency in comparison to the 10 % GL MNs, which were too flexible to penetrate the skin. The histological section results further demonstrated the efficient transdermal delivery of the fluorescent model drug through 0 % GL, 2.5 % GL, and 5 % GL MNs (Fig. 2e). The mechanical performance test revealed that the failure forces of 0 % GL, 2.5 % GL, and 5 % GL MNs were 2.76 ± 0.18 N/needle, 2.10 ± 0.26 N/needle, and 1.74 ± 0.28 N/needle, respectively, further validating the sufficient mechanical strength of MNs (Fig. 2c). Among the MNs containing different GL concentrations, 5 % GL MNs exhibited the fastest dissolution after skin insertion ex vivo and were completely dissolved within 4 min (Fig. 2f and g) owing to the water-absorbing property of GL under the skin. In contrast, both the 2.5 % and 0 % GL MN patches showed more residual MNs after skin application for 4 min (Fig. 2f). The rapid dissolution behavior of 5 % GL MNs was further confirmed by an in vitro drug release test, which showed that 5 % GL MNs exhibited the fastest release rate compared with 0 % or 2.5 % GL MNs (Fig. 2h).

2.2. The antibacterial and anti-inflammatory effects of 5 % GL MN patches in vitro

The fabricated GL MN patch contained conical MNs with a base radius of 200 μm, a height of 850 μm, and a tip radius of ~10 μm, and the MNs were arranged in a 10×10 array in an area of 7 mm × 7 mm (Fig. 3a). The probiotic *L. reuteri* was encapsulated inside the GL MNs with good morphology, as indicated by field-emission scanning electron microscopy (FESEM) images (Fig. 3b and c). Liquid chromatography-mass spectrometry (LC-MS) revealed the presence of a molecular ion
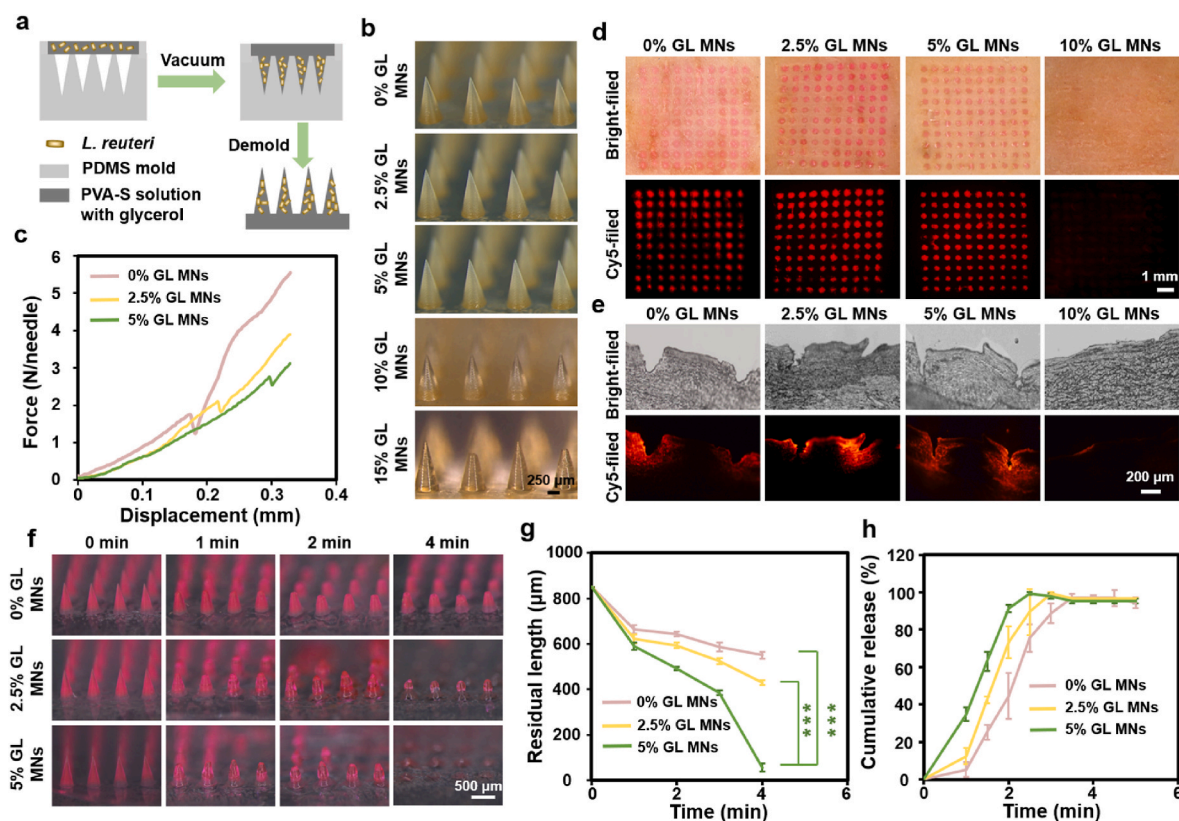

Fig. 2. The fabrication and characterization of GL MN patches. (a) Schematic illustration of the fabrication process of the GL MN patches. (b) Representative bright-field microscopy images of GL MN patches with different glycerol concentrations. (c) Force-displacement curves of the GL MN patches containing 0 %, 2.5 %, and 5 % glycerol, respectively. (d) Representative bright-field and fluorescence-field microscopy images of pig skin after GL MNs insertion. (e) Histological section images of pig skin after application of GL MNs. (f) Representative bright-field microscopy images of residual GL MNs after application to pig skin ex vivo with different application time. g) Quantification of the lengths of residual GL MNs after application to pig skin ex vivo with different application time. (h) Cumulative drug release in vitro from GL MNs in PBS, shown as a function of time. Each point represents mean ± SD (n = 3), ***$P < 0.001$.
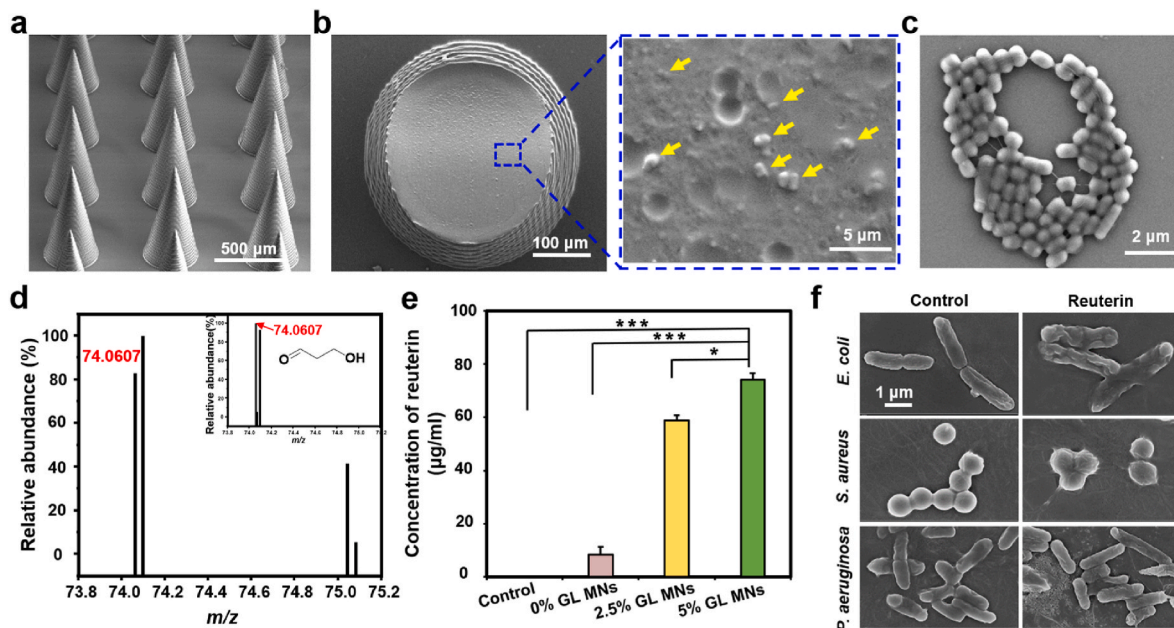
Fig. 3. The characterization of 5 % GL MN patches and the antibacterial effect of reuterin. Representative field emission scanning electron microscopy (FESEM) images of 5 % GL MNs (a), cross-section of one 5 % GL MN (b), and *L. reuteri* extracted from 5 % GL MNs (c). Yellow arrowheads in (b) indicate the existence of *L. reuteri* in MNs. (d) LC-MS analysis of reuterin produced by *L. reuteri* in MNs. (e) Concentrations of reuterin produced by *L. reuteri* that were extracted from different GL MNs and incubated in PBS for 24 h. (f) Representative FESEM images of the morphology of *E. coli*, *S. aureus*, and *P. aeruginosa* with or without reuterin treatment. Each point represents mean $\pm$ SD (n = 3), *$P < 0.05$, and ***$P < 0.001$.

peak ($M^+ = 74.0607$) corresponding to 3-hydroxypropionaldehyde (3-HPA) in the substances produced by *L. reuteri*, which demonstrated the capability of *L. reuteri* to produce the antibacterial agent reuterin (Fig. 3d). Quantitative analysis showed that *L. reuteri* in 5 % GL MNs generated more reuterin than in 0 % and 2.5 % GL MNs (Fig. 3e), owing to the more robust metabolism of GL in 5 % GL MNs. Moreover, *L. reuteri* in GL MNs produced reuterin for more than 9 days (Fig. S1), and the 5 % GL MNs incubation could keep inhibiting the growth of *S. aureus* within the timeframe due to the sustained generation of antibacterial agent reuterin from the probiotics, exhibiting a long-term antibacterial effect of the MN patches (Fig. S2). The produced reuterin caused significant morphological changes in *E. coli*, *S. aureus*, and *P. aeruginosa* in vitro, which are the three most common types of bacteria in wounds (Fig. 3f). The minimum inhibitory concentration (MIC) of reuterin against *E. coli*, *S. aureus*, and *P. aeruginosa* were 29.33 ± 1.69 µg/ml, 20.00 ± 2.45 µg/ml, and 30.00 ± 1.63 µg/ml, respectively (Fig. S3). It has been postulated that reuterin inhibits the activity of bacterial ribonucleotide reductase, which is essential for DNA synthesis, thereby achieving broad-spectrum antibacterial activity [48].

To further evaluate the antibacterial effects of the GL MN patches, we conducted a bacterial viability staining experiment using the SYTO-9/PI assay on *E. coli*, *S. aureus*, and *P. aeruginosa* treated with GL MN patches for 24 h. As shown in Fig. 4a, **b**, and **S4**, all three types of bacteria displayed the lowest viability after incubation with 5 % GL MNs. Additionally, we co-cultured *E. coli*, *S. aureus*, and *P. aeruginosa* with GL MN patches for 24 h on Luria-Bertani (LB) agar plates, and the 5 % GL MN patch exhibited almost completed inhibition of bacterial growth, which was comparable to the antimicrobial efficacy of reuterin (RE) MNs that encapsulated pure reuterin, demonstrating excellent antibacterial property of 5 % GL MNs (Fig. 4c). The optical density at 600 nm (OD_{600}) values, which were obtained by culturing the bacteria in LB liquid medium for 24 h, indicated that nearly no viable bacteria were present after treatment with the 5 % GL MN patch (Fig. 4d). Moreover, when GL MN patches were applied to cultures of *E. coli*, *S. aureus*, or *P. aeruginosa*, the 5 % GL MN patch exhibited the largest inhibition zones, with diameters of 19.77 ± 0.88 mm for *E. coli*, 20.83 ± 1.02 mm for *S. aureus*, and 21.93

± 0.66 mm for *P. aeruginosa*, respectively (Fig. 4e, **f**). Furthermore, the designed 5 % GL MN patch also showed the most efficient clearance of *S. aureus* biofilms in vitro, which generally play critical roles in the drug resistance of harmful bacteria, as demonstrated by confocal laser scanning microscopy (Fig. 5a, **c**) and crystal violet staining (Fig. 5b, **d**). It is worth noting that the 5 % GL MN patch showed a biofilm clearance outcome similar to that of the RE MN patch, without any significant difference (Fig. 5c and d). These results indicate that the primary factor that led to the satisfactory antimicrobial effect of the 5 % GL MN patch was probably the generation of the antibacterial compound reuterin, which is consistent with conclusions reported in the literature [26,48, 49].

The anti-inflammatory effect of the probiotic-based living MN patch was also investigated in vitro. RAW 264.7 cells were incubated with the supernatant of liquid medium that had cultured *S. aureus* or the mixture of *S. aureus* and *L. reuteri*-loaded MN patch for 24 h. Subsequently, CD86 expression that is generally used as the indicator of M1 macrophages, was measured by flow cytometry after another 24 h. As shown in Fig. 6a–c, the expression of CD86 was significantly down-regulated on RAW 264.7 cells (changing from 11.41 ± 0.69 % to 8.50 ± 0.18 %, $p < 0.01$), which was probably ascribed to the growth inhibition of the harmful bacteria and decrease of the secreted toxin (Fig. 6b), indicating a good anti-inflammatory effect of the probiotic-based MN patch. The anti-inflammatory effect of the 5 % GL MN patch was also validated by the results of real-time quantitative polymerase chain reaction (qPCR) (Fig. 6d, **e**) and western blotting (Fig. 6f–h), respectively, which determined that the use of the MN patch could significantly reduce the expression level of IL-6 and TNF-α in RAW 264.7 cells.

Collectively, these results demonstrated that 5 % GL MNs provided good protection for the loaded probiotic *L. reuteri*, which displayed active GL metabolism and robust reuterin production, thereby endowing the MN patch with superior antibacterial and anti-inflammatory properties.
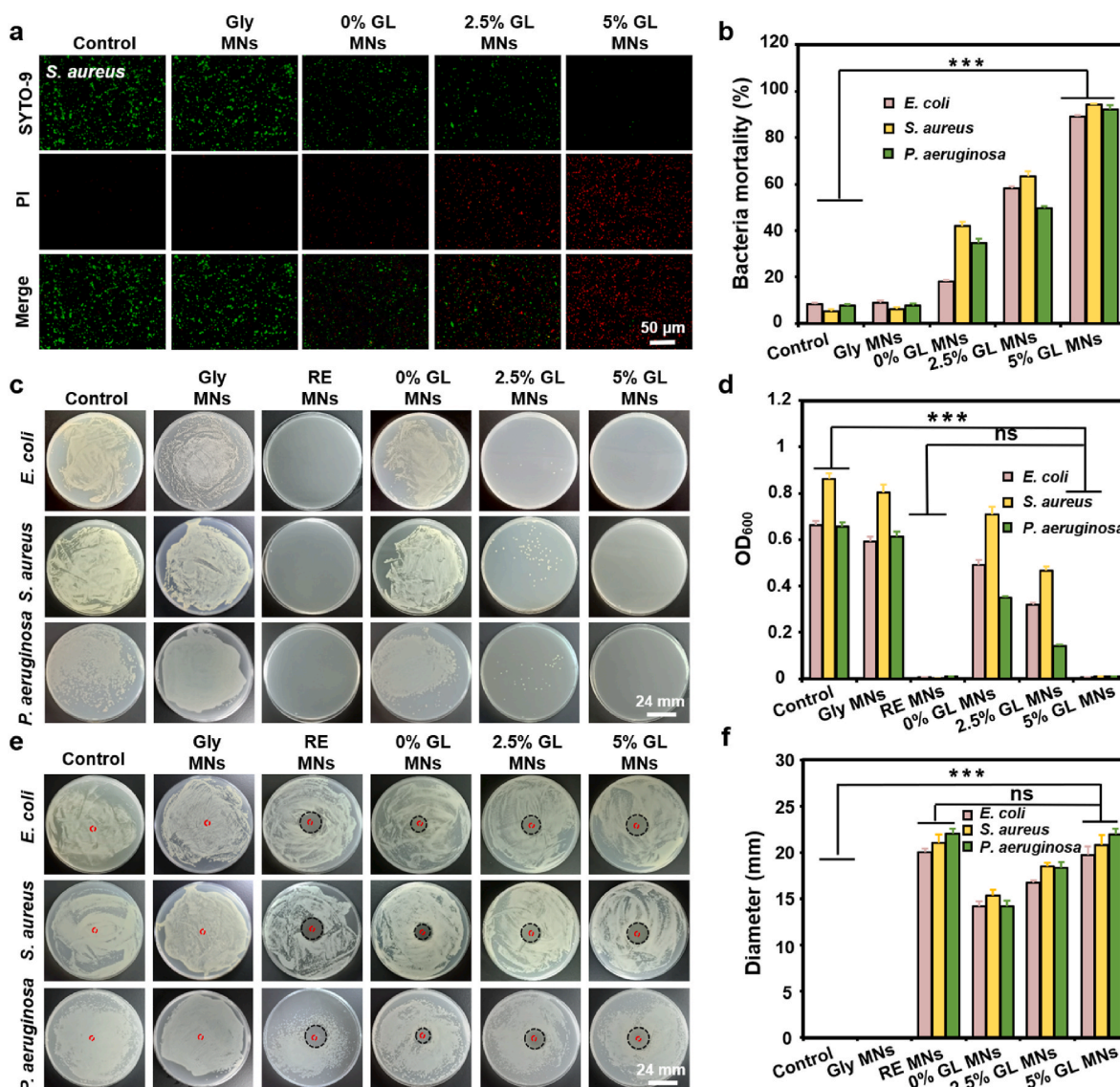
Fig. 4. The antibacterial effect of 5 % GL MNs in vitro. (a) Live/dead assay of *S. aureus* after incubation with Gly MNs (MNs containing 5 % glycerol but without the probiotic of *L. reuteri*) or GL MNs containing different glycerol concentrations for 24 h. (b) Bacteria mortality of *E. coli*, *S. aureus*, and *P. aeruginosa* after being treated with Gly MNs or GL MNs containing different glycerol concentrations. (c) Representative bright-field images of LB agar plates showing the growth of *E. coli*, *S. aureus*, and *P. aeruginosa* after incubation with different MNs for 24 h. (d) The OD_{600} values of *E. coli*, *S. aureus*, or *P. aeruginosa* in LB liquid medium after receiving different MN treatments for 24 h. (e) Representative bright-field images of inhibition zones against *E. coli*, *S. aureus*, or *P. aeruginosa* with different MN treatments for 24 h. Red dashed circles indicate the position of the drug-sensitive paper; black dashed circles indicate inhibition zones. (f) Diameter of the inhibition zones against *E. coli*, *S. aureus*, or *P. aeruginosa*. Each point represents mean ± SD (n = 3), ***$P < 0.001$. The ns indicates no significance.

2.3. The biocompatibility and stability assay of 5 % GL MN patches in vitro

Based on the characterization of the GL MN patches in terms of morphology, skin penetration ability, mechanical strength, dissolution speed, and antibacterial efficacy, the 5 % GL MN patch was determined to be the optimal formulation for delivering *L. reuteri* to wounds for antibacterial purposes. To evaluate the cytotoxicity of the 5 % GL MN patch, a calcein/PI (propidium iodide) staining kit was used to analyze cellular viability after incubation of NIH-3T3 cells (Fig. 7a) or human umbilical vein endothelial cells (HUVECs) (Fig. S5) with the 5 % GL MN patch, reuterin, PVA/sucrose, or 5 % glycerol for 24 h. As shown in Fig. 7a and **b**, incubation with either the 5 % GL MN patch or the individual components did not show any significant difference in cell viability compared to the control group that did not receive any treatment, indicating the satisfactory biocompatibility of the 5 % GL MN

patches. To investigate whether excess reuterin produced by *L. reuteri* causes toxicity in normal tissue cells, NIH-3T3 cells or HUVECs were incubated with different concentrations of reuterin for 24 h. As shown in Fig. S6, both cells still maintained over 95 % cell viability even at a concentration as high as 100 μg/ml of reuterin. Additionally, the hemolysis assay showed that the incubation of red blood cells with PVA-sucrose (PVA-S), GL, or *L. reuteri* resulted in a negligible hemolysis rate (Fig. S7). Collectively, these results demonstrate the excellent biocompatibility of the 5 % GL MN patches in vitro.

The stability of *L. reuteri* in a 5 % GL MN patch is critical for maintaining its antibacterial activity. To assess the viability of *L. reuteri* in a 5 % GL MN patch, we stored the 5 % GL MN patches at room temperature and 4 °C, respectively, and then measured the survival rate of *L. reuteri*. The viability results showed that the probiotic could survive in the 5 % GL MN patch for 7 days at room temperature, with over 40 % of the living bacteria remaining in the patch (Fig. 7c, **d**). Notably, when the
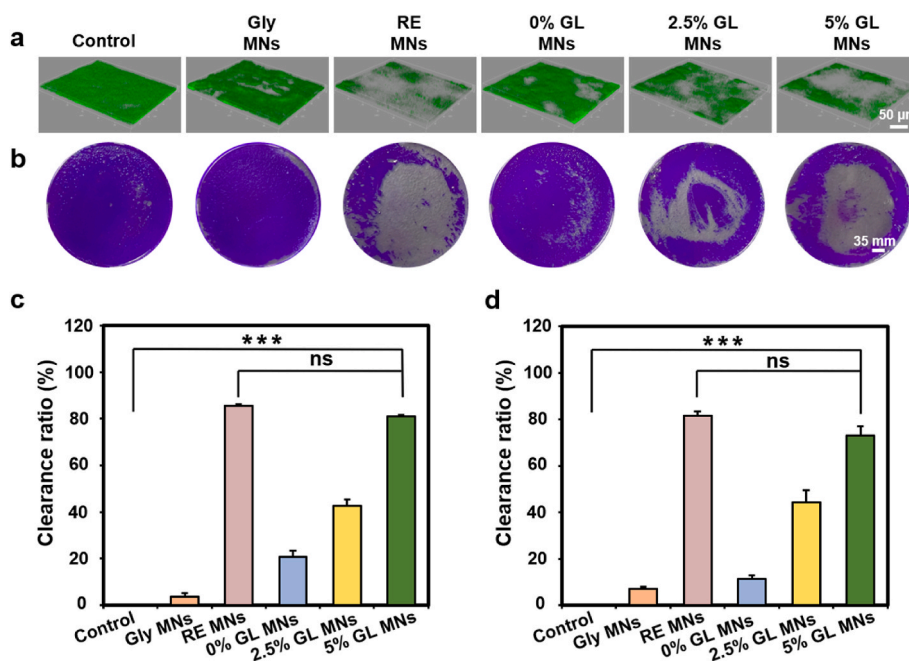
Fig. 5. The biofilm clearance effect in vitro of GL MN patches. (a) Confocal laser scanning microscopy of *S. aureus* after receiving different treatments. Green: live bacteria. (b) Pictures of biofilms stained with crystal violet after being treated with different MNs. (c) Biofilm clearance ratio of *S. aureus* after receiving different treatments in (a). (d) Biofilm clearance ratio of *S. aureus* after being treated with different MNs in (b). Each point represents mean ± SD (n = 3). *$P < 0.05$, **$P < 0.01$, and ***$P < 0.001$. The ns indicates no significance.

MN patch was placed at 4 °C, the beneficial bacteria maintained a high viability (>80 %) inside the MNs after 60 days, and about 50 % *L. reuteri* still kept active for as long as 90 days, indicating long-term stability of the probiotic inside 5 % GL MN patches (Fig. 7e, **f**). The great stability of the 5 % GL MN patches in vitro was further validated by the live/dead staining of the probiotics inside MNs, which exhibited that *L. reuteri* could keep a high viability (~90 %) in the MN patches after keeping the MN patches for 30 days at 4 °C (Fig. S8). In addition, there was no significant difference in bacterial viability between the 5 % GL MN patches and 0 % GL MN patches (Fig. 7d, f), suggesting that the addition of glycerol to the MN patches did not affect the activity of the probiotic.

2.4. Wound healing promotion of 5 % GL MN patches in vivo

S. aureus is the most common pathogenic species in chronic wounds [50,51]. It has been reported that a full-thickness skin excision wound on a rodent, for example mouse, is very clinically relevant [52,53]. Therefore, to further assess the antibacterial effect and therapeutic efficacy of the designed MN patches in promoting wound healing, we established a full-thickness skin wound model (diameter: 1 cm) with *S. aureus* infection on the backs of mice. Two days later, the mice were randomly divided into five groups and treated with: 1) no treatment (Control), 2) MN patches loaded with reuterin (RE MNs), 3) MN patches made of a PVA-sucrose matrix (PVA-S MNs), 4) MN patches loaded with *L. reuteri* but without glycerol (0 % GL MNs), and 5) MN patches loaded with *L. reuteri* and 5 % glycerol (5 % GL MNs) (Fig. 8a and b). Images of the wounds were taken for each group on days 0, 3, 5, 7, and 9 (Fig. 8b), and wound size changes over time were analyzed using a simulation method (Fig. 8c). The *L. reuteri*-encapsulated MNs could rapidly dissolve within 4 min after the application in the wound tissue, thereby successfully delivering the probiotic to the wound site with a high delivery efficiency (Fig. S9). The analysis of wound areas showed that wounds treated with 5 % GL MNs experienced accelerated recovery, and the wound size was only 0.69 % ± 0.12 % on day 9, compared to 11.83 % ± 1.38 %, 8.51 % ± 1.27 %, 8.70 % ± 0.14 %, and 5.82 % ± 0.82 % in the other groups, respectively, which indicated that infections caused by

S. aureus were well controlled in the 5 % GL MNs group (Fig. 8e).

To confirm the antibacterial efficacy of 5 % GL MNs in mice, *S. aureus* was isolated from the wound on days 0, 3, 5, 7, and 9 and then cultured on LB agar plates (Fig. 8d). Compared with the other groups, wounds treated with 5 % GL MNs showed no presence of *S. aureus* at 3 days post-treatment, revealing the superior antimicrobial efficiency of 5 % GL MNs in vivo (Fig. 8f). It is worth noting that the wounds treated with RE MNs or 0 % GL MNs inhibited the growth of *S. aureus* at the early stage (i.e., day 3), but the number of bacteria in the wounds increased starting from day 5 (Fig. 8d, f), largely because of the consumption of existing reuterin, indicating that 5 % GL MNs were capable of effectively eliminating *S. aureus* from wounds through the continuous metabolism of glycerol and constant production of reuterin via the probiotic *L. reuteri*. The concentration of glycerol in mice decreased over time post the administration of the MN patch due to the gradual metabolism by the probiotics at the wound site (Fig. S10). The survival result of the delivered *L. reuteri* showed that the probiotic could exist and maintain its activity at the wound site for 9 days, further validating the long-term antimicrobial activity during the wound healing period (Fig. S11). The adhesion and colonization of *L. reuteri* under the skin was verified by the gram staining of the beneficial bacteria (Fig. S12). In addition, the body weights of the mice were monitored during the wound healing process, and the results showed no significant changes in any of the treatment groups (Fig. 8g), indicating good biosafety of the 5 % GL MN patches in vivo. Moreover, the skin of the mice recovered rapidly after the application of the 5 % GL MN patches without causing any apparent skin irritation (Fig. S13). The skin condition of mice was also carefully examined for 30 days. As shown in Fig. S14, the skin did not show any redness, swelling or itching within one month, indicating that transdermal delivery of *L. reuteri* did not cause negative effects in animals. Collectively, these results suggested satisfactory biocompatibility and biosafety of the MN patches in vivo.

2.5. Therapeutic efficacy of 5 % GL MN patches in vivo

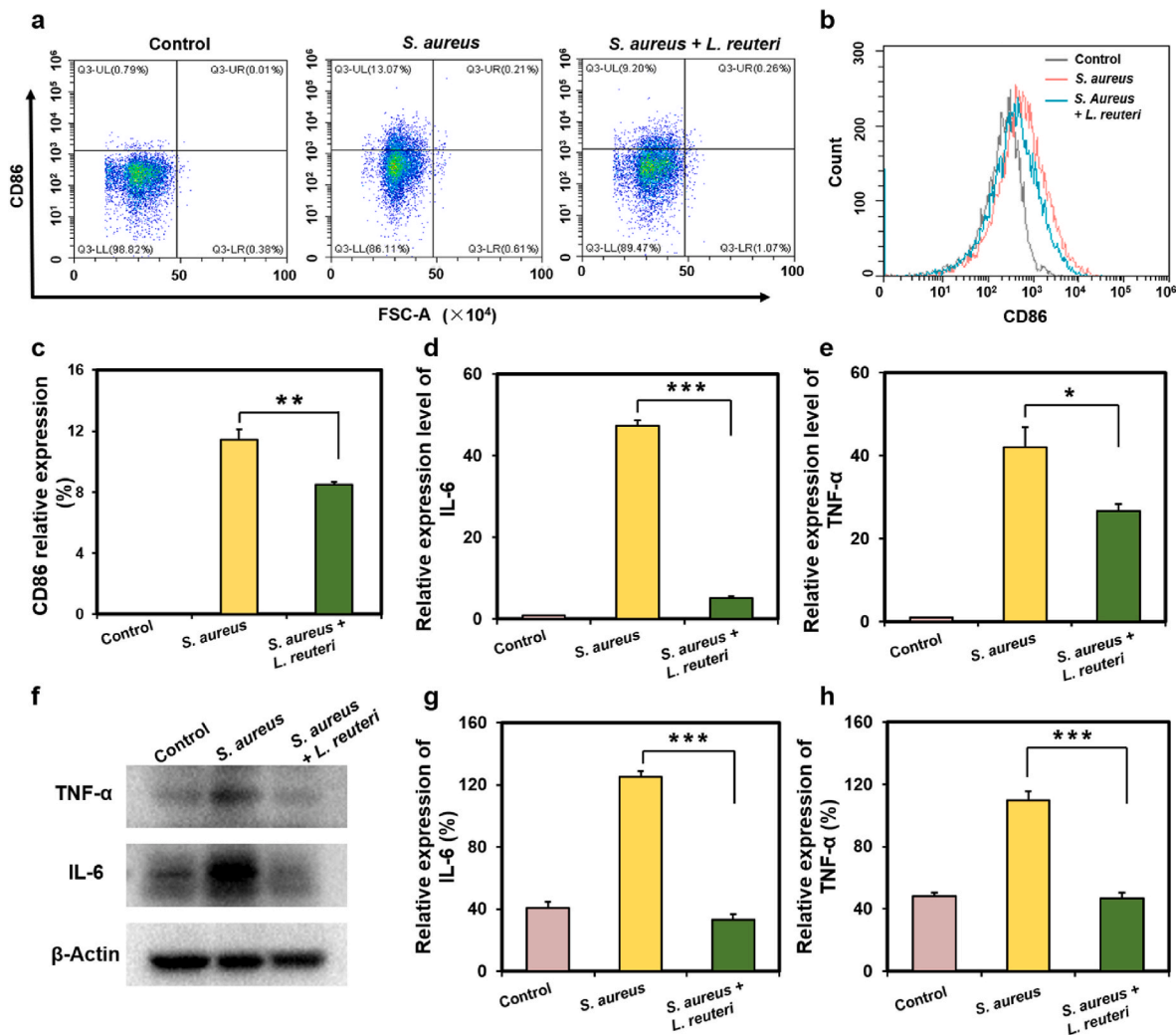To further confirm the therapeutic efficacy of the 5 % GL MN patches

Fig. 6. The anti-inflammatory property of the GL MNs patch in vitro. (a) Intracellular CD86 fluorescence intensity of RAW 264.7 with different groups analyzed by flow cytometry. (b) Flow cytometry histogram of different groups. (c) CD86 relative expression of different groups. (d–e) Expression levels of IL-6 and TNF-α in the RAW 264.7 cells determined by real-time qPCR after different treatments. (f–h) Expression levels of IL-6 and TNF-α in the RAW 264.7 cells determined by western blotting after different treatments. Each point represents mean ± SD (n = 3), *$P < 0.05$, **$P < 0.01$, and ***$P < 0.001$.

in accelerating wound healing, we evaluated tissue regeneration at the wound site after MN patch treatment. Hematoxylin and eosin (H&E) staining showed that the wounds treated with 5 % GL MNs exhibited almost complete closure on day 9 (Fig. 9a), and the length (Fig. 9e) and thickness (Fig. 9f) of the granulation tissue in the wounds were significantly smaller than those in the other groups. Collagen, a key component of damaged skin tissue, plays a crucial role in wound healing and tissue remodeling [54]. Masson's staining revealed that the wounds treated with 5 % GL MNs had more collagen deposition on day 9 (Fig. 9b), with a collagen volume fraction (CVF) of 68.37 % ± 0.23 %, significantly higher than that in the other groups (Fig. 9g). In addition, immunohistochemical staining for interleukin-6 (IL-6) demonstrated that the application of 5 % GL MNs alleviated inflammation at the wound site, with much lower IL-6 secretion than in the other groups (Fig. 9c, h), indicating a strong anti-inflammatory effect of 5 % GL MNs. Angiogenesis is a critical step in wound healing and tissue remodeling, and CD31 plays a vital role in angiogenesis as a marker of blood vessel formation [54]. Immunofluorescent staining for CD31 displayed that the microvessel density at the wound site was significantly higher in the 5 % GL MNs group, reaching 8.1 % ± 0.14 % (Fig. 9d, i), which suggested that 5 % GL MNs possessed the ability to promote angiogenesis at wounds. Furthermore, H&E staining of the major organs of the treated mice showed that these organs maintained good integrity without any

significant damage or defects compared to normal tissues (Fig. S15), suggesting satisfactory biocompatibility of 5 % GL MNs in vivo. Additionally, serum levels of alanine aminotransferase (ALT), total bilirubin (TBIL), blood urea nitrogen (BUN), and creatinine (CR) were analyzed to evaluate liver and kidney functions after the mice received different treatments, which showed no significant difference between the MN patch group and the control group (Fig. S16), further demonstrating the great biosafety of the MN patches.

3. Discussion

In summary, we developed a novel and biocompatible probiotic-based MN patch with a long-acting antimicrobial effect to promote healing of infected wounds. The MNs provided good protection for the probiotic, and it maintained a viability as high as 80 % inside the solid MNs for more than 60 days at 4 °C. Upon insertion, MNs quickly dissolved and achieved rapid delivery of the beneficial bacteria in deep wound tissue, where the probiotic was capable of surviving in the wound for approximately one week and continuously converting the co-delivered glycerol into antimicrobial substances, thereby achieving a long-acting antibacterial effect in the infected wound. In a mouse model of *S. aureus*-infected wounds, one administration of the probiotic-based MN patch exhibited a superior effect in eliminating harmful bacteria and
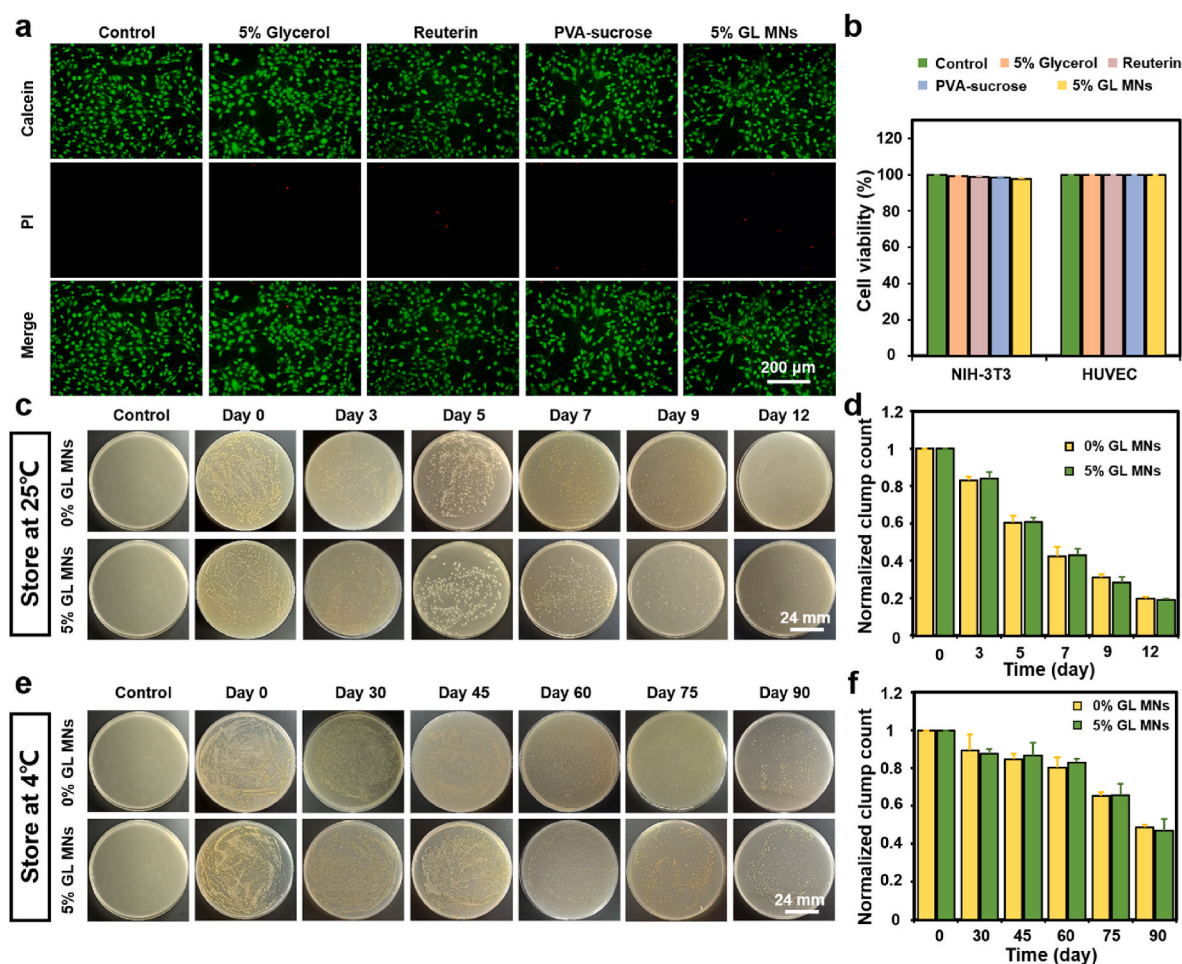
Fig. 7. Cytotoxicity and stability of 5 % GL MNs. (a) Live/dead assay of NIH-3T3 cells after receiving different treatments. (b) Cell viability analysis of NIH-3T3 cells and HUVECs after receiving different treatments. Bright-field images of MRS agar plates showing the viability of *L. reuteri* after storing 0 % and 5 % GL MN patches at 25 °C (c), or 4 °C (e) over time. The clump count of *L. reuteri* in GL MNs normalized to day 0 after being stored for different times at 25 °C (d), or 4 °C (f). Each point represents mean ± SD (n = 3).

promoting wound closure with reduced inflammation and enhanced tissue regeneration and angiogenesis compared with the control groups, suggesting great potential for the treatment of chronically infected wounds.

Although some MN patches that possess similar properties, such as antibacterial and anti-inflammatory activities, have been reported for accelerating infected wound healing [55–57], the designed MN patch has some unique features compared with those reported systems. First, the fabrication is easy and only involves the encapsulation of probiotic in soluble matrix, which will greatly facilitate to scale up the MN patch production. Second, to achieve long-acting antibacterial effect for promoting wound closure, we only use probiotic that is naturally present in the human body. Therefore, not like other MN patches that usually contain some metal ions or chemicals with uncertain safety, the application of the MN patch does not bring any toxic solvent or other components, thereby owning satisfactory biocompatibility and biosafety.

This study has a few limitations. First, the designed MN patch only showed satisfactory therapeutic outcomes and biocompatibility for the treatment of infected wounds in a mouse model; its therapeutic efficacy and biosafety need to be validated in larger animals. Additionally, the activity of probiotics in vivo is worth examining after transdermal delivery via the MN patch, which can be achieved in the future using special probes that can directly detect or visualize beneficial bacteria in the wound.

This project aims to develop a self-administered, effective, and biosafe MN patch for treating infected wounds. Currently, the MN patch can maintain high viability of the probiotics for more than two months at low temperatures, but it will be more attractive to maintain good activity of the beneficial bacteria for an extended period under mild conditions, such as at room temperature, which can probably be accomplished by the use of novel materials or more advanced fabrication technologies. Moreover, it will be necessary to develop a mechanism for the MN patch, such as a color change or sound notification, which can provide feedback to patients when they successfully administer the MN patches on themselves.

4. Materials and methods

4.1. Materials

PVA (Mw, 9000–10000 Da) was purchased from Sigma-Aldrich (USA). Sucrose, DL-Tryptophan, 3-HPA, and gelatin were purchased from Macklin (Shanghai, China). Glycerol and hydrochloric acid (12 mol/l) were purchased from SCR (Shanghai, China). The MRS broth was obtained from HKM (Guangdong, China). LB nutrient agar and LB broth were purchased from HopeBio (Qingdao, China). The SYTO-9/PI live/dead bacterial double-staining kit was purchased from Maokangbio (Shanghai, China). Dulbecco's Modified Eagle's Medium (DMEM), fetal bovine serum (FBS), and penicillin-streptomycin double antibiotics were purchased from Gibco (USA). A live/dead cell staining kit was purchased from Beyotime (Shanghai, China). Phosphate-buffered saline (PBS) was purchased from Service Bio (Wuhan, China). Rhodamine B was
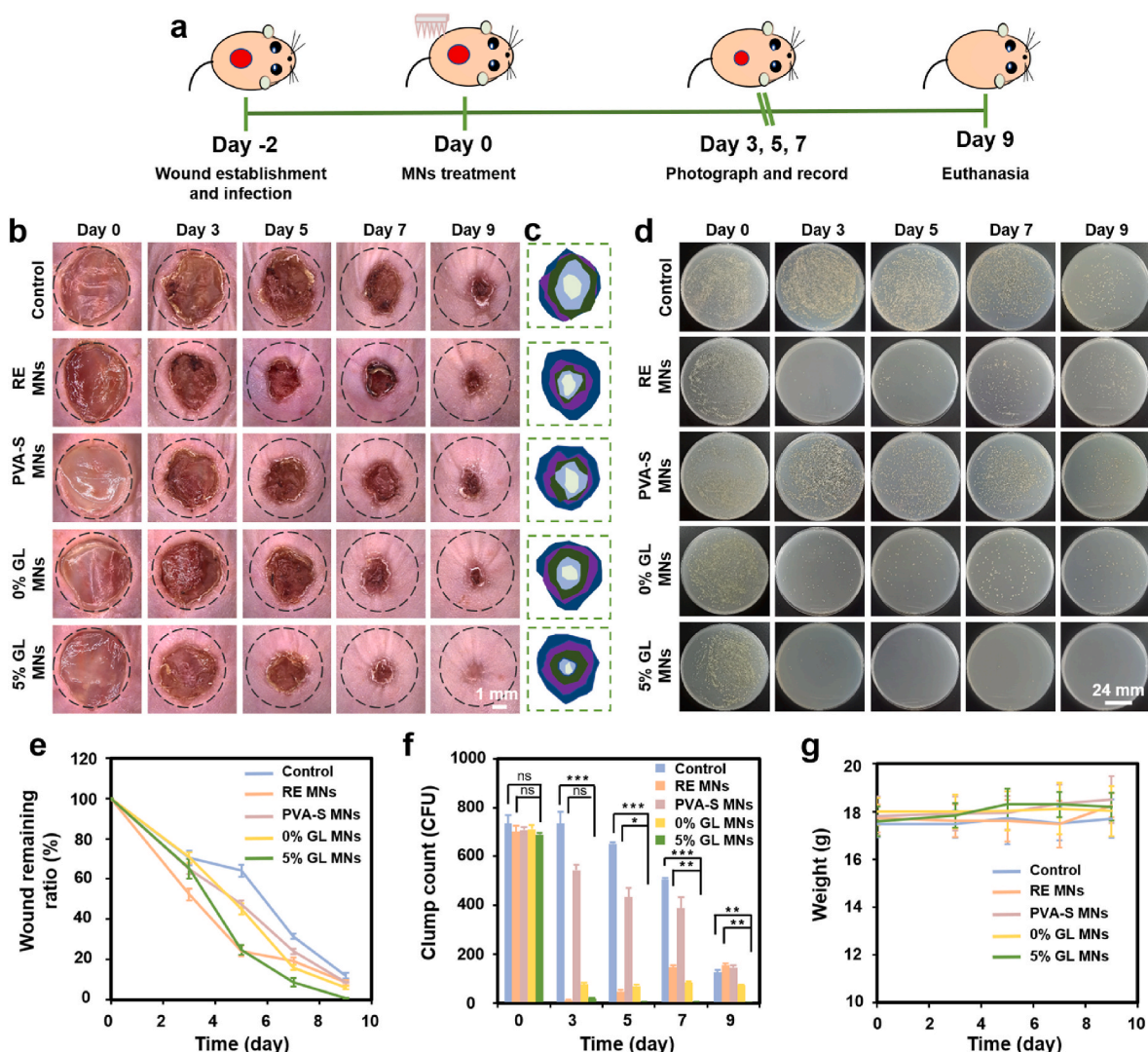
Fig. 8. Antibacterial effect of 5 % GL MN patches in vivo. (a) Time scheme of the experiment in vivo. (b) Representative pictures of the mice skin wounds on days 0, 3, 5, 7, and 9 after receiving different treatments. Black dashed circles indicate the original wound area (diameter: 1 cm). (c) Schematic diagram of wound morphological changes in different groups within 9 days. (d) Representative pictures of *S. aureus* that were separated from wound tissue on days 0, 3, 5, 7, and 9 in different groups. (e) Wound remaining ratio-time curves of the mice skin wounds with different treatments. (f) Clump count of *S. aureus* that was separated from wound tissue on days 0, 3, 5, 7, and 9 in different groups. (g) Body weight changes of the mice after receiving different treatments. Each point represents mean ± SD (n = 7), $*P < 0.05$, $**P < 0.01$, and $***P < 0.001$. The ns indicates no significance.

purchased from Solarbio (Beijing, China).

4.2. Bacteria and cell lines

L. reuteri ATCC 53608 was purchased from the Shanghai Bioresource Collection Center (Shanghai, China) and cultured in MRS nutrient broth. The *E. coli*, *S. aureus*, and *P. aeruginosa* bacteria were obtained from the American Type Culture Collection (ATCC, Rockville, MD, USA) and cultured in LB nutrient broth. NIH-3T3 and HUVEC cell lines were purchased from Procell Biological Co., LTD (Wuhan, China). The cells were cultured in DMEM supplemented with 10 % FBS and 1 % penicillin-streptomycin at 37 °C with 5 % CO_2.

4.3. Characterization of L. reuteri and the GL MN patches

The *L. reuteri* morphology and the microstructure of the 5 % GL MN patches were observed using FESEM (Carl Zeiss, Zeiss GeminiSEM 500) with gold sputtering. The mechanical strengths of the GL MN patches were tested using a force-measurement system (Mark-10, ESM303).

Fluorescent images were captured using an inverted fluorescence microscope (Olympus, IX73). Images were captured using an optical microscope (Leica TL3000 Ergo).

4.4. Fabrication of the MN patches

Polydimethylsiloxane (PDMS) (Dow Corning, Midland, USA) molds were used to fabricate the MN patches. A mixture was prepared by mixing 10^9 CFU/ml *L. reuteri* with 18 % (w/v) PVA, 18 % (w/v) sucrose, and 5 % (v/v) glycerol that were dissolved in MRS medium. One hundred microliters of the mixture were add to the surface of the PDMS mold, which was kept on top of a vacuum chuck for 2 h with the vacuum of −2.2 MPa. The mold was then placed in a desiccator at room temperature for two days for complete drying. Finally, the MN patch was carefully peeled from the mold and stored safely in a desiccator until further use. For the fabrication of 0 %, 2.5 %, 10 %, and 15 % GL MN patches, the preparation method was the same as that for the 5 % GL MN patches, except for the use of different concentrations of glycerol.
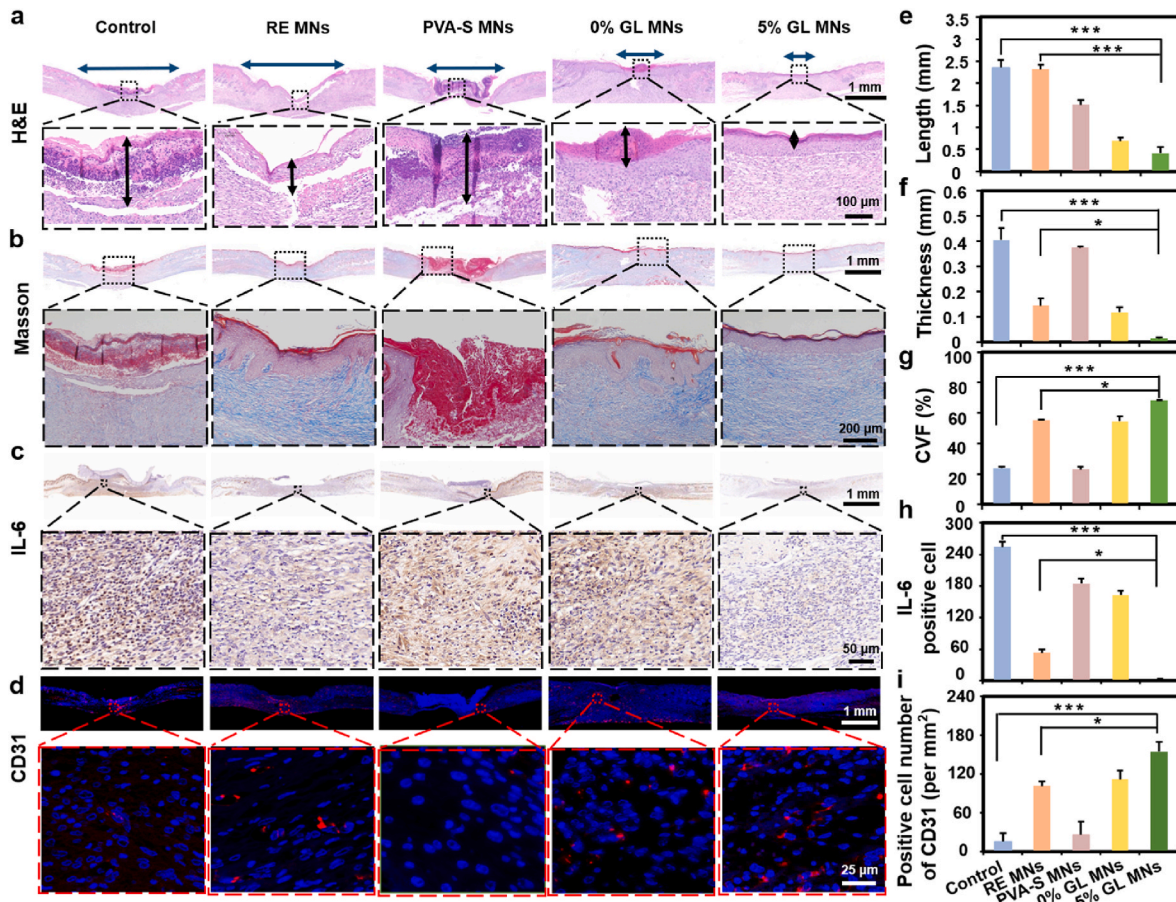
Fig. 9. Investigation of tissue regeneration, inflammatory response, and angiogenesis after different treatments. Representative bright-field microscopy images of H&E staining (a), Masson staining (b), and immunohistochemistry staining of IL-6 (c) after different treatments on day 9. Blue arrows in (a) indicate the wound length, and black arrows in (a) indicate the wound thickness. (d) Immunofluorescence images of neovascularization in wound tissue after being stained with CD31 (red) and DAPI (blue) after different treatments on day 9. Analysis of wound length (e), and wound thickness (f) shown by H&E staining for different treatments on day 9. (g) The collagen volume fraction (CVF) for different treatments on day 9. (h) Positive cells shown by immunohistochemistry staining for IL-6 for different treatments on day 9. (i) The relative coverage area of CD31 for different treatments on day 9. Each point represents mean $\pm$ SD (n = 7), *$P < 0.05$, **$P < 0.01$, and ***$P < 0.001$.

4.5. Application of MN patches to pig skin in vitro

GL MN patches loaded with Rhodamine B as a model drug were applied to pig skin ex vivo for 4 min. The applied skin and residual MN patches were observed by fluorescence microscopy under bright-field and Cy5-field. After that, the skin was cut into 10 μm-thick slices using a cryostat (Thermo Fisher Scientific, HM525 NX) for histological analysis.

4.6. In vitro release from MN patches

Rhodamine B was added to the MN patches as a model drug to mimic the in vitro release of *L. reuteri* in the MN patches. The MN patch was placed in 2 ml PBS solution (pH 7.4), and 0.5 ml samples were taken at 0.5, 1, 1.5, 2, 2.5, 3, 3.5, 4, 4.5, and 5 min, followed by supplementation with 0.5 ml fresh PBS solution to keep the volume constant. The UV–visible absorbance of the samples was measured at 552 nm using a UV spectrophotometer (Shimadzu, UV-2600) to calculate the cumulative drug release. The cumulative model drug release percentage was analyzed by dividing the cumulative amount released by the total drug dosage in the MN patch.

4.7. Dissolution rate of MN patches in skin ex vivo

The MN patches were inserted into the excised porcine skin and

removed at 1, 2, and 4 min. The lengths of the MNs after skin removal at different time points were observed and photographed using an optical microscope, followed by measurements using ImageJ software.

4.8. Qualitative and quantitative analysis of reuterin

The probiotic of *L. reuteri* was separated from the MRS liquid medium by centrifugation at 4500 r/min for 5 min, and then dispersed in a mixture of 4 ml sterilized ddH$_2$O and 200 μl glycerol. After being incubated at 37 °C for 24 h, the supernatant was collected by centrifugation at 1000 r/min for 10 min, which was used as the test sample. The test sample, along with a standard sample of reuterin at the concentration of 100 μg/ml, were analyzed using LC-MS (Thermo Fisher Scientific, Q Exactive Focus). The concentration was determined using a colorimetric method. After mixing 300 μl hydrochloric acid (12 M) and 75 μl DL-tryptophan solution that were dissolved in 0.05 M hydrochloric acid (0.01 M) and 100 μl 3-HPA with different concentrations of 1000, 500, 250, 125, and 62.5 μg/ml, the absorbance at 560 nm was obtained using a UV–visible spectrophotometer to plot the standard curve. The concentrations of reuterin produced by *L. reuteri* from the different GL MNs were determined using the same method.

4.9. Bacterial morphology observation

Changes in bacterial morphology were investigated after different

treatments. For the control group, *S. aureus* was separated from the LB liquid medium by centrifugation at 4500 r/min for 5 min after being cultured for 24 h, followed by dispersion in 1 ml PBS. For the treatment group, *S. aureus* was incubated with 1 ml PBS and 100 µl of 100 µg/ml reuterin at 37 °C for 12 h, and the bacteria were collected by centrifugation at 4500 r/min for 5 min. The treated *S. aureus* cells were then fixed with 1 ml of 2.5 % glutaraldehyde overnight, washed twice with 2 ml saline, and once with 2 ml ddH$_2$O. The bacteria were then dehydrated with 50 %, 70 %, and 90 % ethanol for 15 min and then dispersed with absolute ethanol. Finally, the morphology of *S. aureus* was observed using FESEM on silicon slides. The same procedure was followed for *E. coli* and *P. aeruginosa*.

4.10. Antibacterial effect of reuterin on S. aureus

To investigate bacterial viability after treatment with reuterin collected from the GL MN patches, the staining reagent was prepared by mixing SYTO-9 and PI staining reagents with PBS at a ratio of 1:1:1500. Simultaneously, *L. reuteri* extracted from GL MN patches was cultured in MRS liquid medium with the addition of 2.5 % and 5 % glycerol (2.5 % GL MN and 5 % GL MN), and in MRS liquid medium without glycerol (0 % GL MN) at 37 °C for 24 h. The cultures were then centrifuged at 4500 rpm for 5 min, and the supernatant was collected and reuterin concentrations of 8.19 µg/ml, 59.38 µg/ml, and 74.73 µg/ml were obtained, respectively. These solutions were used in subsequent experiments. Then, 100 µl of reuterin obtained from each GL MN patch and *S. aureus* (10^9 CFU) were added to 1 ml PBS, followed by incubation at 37 °C for 12 h. After centrifuging the solution at 4500 r/min for 5 min to remove the supernatant, 100 µl of the staining reagent was added to resuspend the bacteria. Then, *S. aureus* was incubated in the dark for 15 min, and washed once with 100 µl PBS. Finally, 100 µl PBS was added to disperse the bacteria. Fluorescence images were obtained under an inverted microscope using FITC and CY5 channels at 60 × magnification. The same procedure was followed for *E. coli* and *P. aeruginosa*. Bacterial mortality was analyzed by dividing the number of dead bacteria by the total number of bacteria.

$$Bacteria\ mortality = \frac{Dead\ bacteria\ count}{Total\ bacteria\ count} \times 100\%.$$

4.11. Antibacterial effect of GL MN patches in vitro

To further investigate the antibacterial effect of the GL MN patches in vitro, 5×10^5 CFU/ml *S. aureus* was incubated with one MN patch from each group (Control, RE MNs, 0 % GL MNs, 2.5 % GL MNs, and 5 % GL MNs) at 37 °C for 24 h. After that, the absorbance value of bacterial solution at 600 nm was measured using a UV spectrophotometer, and 20 µl culture solution was inoculated into LB solid medium to observe colony growth. The same procedure was followed for *E. coli* and *P. aeruginosa*. Each group was comprised of three replicates.

4.12. Determination of the inhibition zone

Reuterin extracted from each group (Control, RE MNs, 0 % GL MNs, 2.5 % GL MNs, and 5 % GL MNs) was applied to drug-sensitive papers. Meanwhile, 20 µl of *S. aureus* culture solution with the concentration of 10^8 CFU/ml was inoculated into LB solid medium. The drug-sensitive papers were then placed in the center of the LB solid medium and incubated at 37 °C for 24 h, after which the diameter of the inhibition zone was measured. The same procedure was followed for *E. coli* and *P. aeruginosa*. Each group was comprised of three replicates.

4.13. Biofilm clearance experiment

The bacterium of *S. aureus* was cultured in LB medium containing 3 % sucrose for 48 h to form the biofilm. The biofilm was incubated in fresh LB medium containing the corresponding MN patch for 12 h. After that, the supernatant was removed, the biofilm was cleaned once with PBS and fixed with methanol for 30 min. After fixation, 0.1 % crystal purple was applied for 30 min to stain biofilm. The biofilm was photographed, dissolved in 33 % glacial acetic acid, and the absorbance at 595 nm was measured using an ultraviolet spectrophotometer to calculate the clearance rate of the biofilm. At the same time, after co-incubation for 12 h, the biofilm was stained with the SYTO-9 staining reagent for 15 min, and then photographed with the laser confocal microscope, and the clearance rate of the biofilm was calculated according to the area of the biofilm removed.

4.14. Hemolysis experiment

To examine the biosafety of GL MN patches, 1 ml blood was collected from each mouse and placed in a tube containing sodium heparin. The tube was then washed five times with 3 ml saline solution (gently agitated and centrifuged at 1500 rpm for 10 min) until the supernatant became clear. Red blood cells were dispersed in 3 ml saline solution and divided into the following groups: ddH$_2$O, saline, PVA-sucrose, PVA-sucrose + glycerol, PVA-sucrose + *L. reuteri*, and PVA-sucrose + glycerol + *L. reuteri* (ddH$_2$O, saline, PVA-S, PVA-S + GL, PVA-S + LR, PVA-S + GL + LR). The MN patches from each group were then added to the red blood cell suspension and incubated overnight. After centrifugation at 1500 rpm for 10 min, the supernatant was collected and the absorbance at 540 nm was measured to calculate the hemolysis rate of the cells. Each group was comprised of three replicates.

4.15. Investigation of microporous healing in vivo

First, the mice (~20 g) were anesthetized with sodium pentobarbital, and the dorsal fur of the mice was removed. Subsequently, 5 % GL MN patches were applied to the skin of the mice. The skin on the dorsal area of the mice was observed under a stereomicroscope to evaluate the healing condition of the skin before and at 0, 2, 5, 10, and 15 min after the MN patch application.

4.16. Cell viability staining experiment

To validate the biocompatiblity of MN patches, NIH-3T3 or HUVEC cells were incubated with DMEM containing 100 µl reuterin (40 µg/ml), 100 µl of 18 % PVA-sucrose, 100 µl of 5 % glycerol solution, or a 5 % GL MN patch (RE, PVA-S, 5 % GL, 5 % GL MN) at 37 °C for 24 h. After removing the culture medium, calcein-AM/PI reagent mixed with DMEM cell culture medium at a ratio of 1:1000 was added to the NIH-3T3 cells and HUVECs. The cells were then incubated at 37 °C for 20 min. Excess staining reagents were washed with PBS and replaced with the same volume of DMEM culture medium. Cell staining was then observed under a fluorescence microscope in the FITC and CY5 channels.

4.17. In vitro cytotoxicity assay of reuterin

The toxicity of reuterin in NIH-3T3 cells and HUVECs was determined using the CCK-8 assay. A culture medium containing 100, 50, 25, 12.5, 6.25, 3.125, or 0 µg/ml reuterin was prepared by mixing the determined volume of reuterin (10 mg/ml) with DMEM culture medium. Next, culture medium was added to adherent NIH-3T3 cells or HUVECs, with five replicate wells per group. The cells were incubated for 24 h, after which the reuterin-containing medium was removed. Fresh 100 µl DMEM culture medium mixed with 10 µl CCK-8 solution was added to each well, and incubated at 37 °C for 1 h. The absorbance of each well was measured at 450 nm using a microplate reader, and cell viability was calculated based on the absorbance.

4.18. Stability and survival test of L. reuteri in 5 % GL MN patches in vitro and in mice in vivo

The 5 % GL MN patch that contained *L. reuteri* was stored in a sealed container at room temperature (i.e., 25 °C). On days 0, 3, 5, 7, 9, and 12, the 5 % GL MN patch was dissolved in 0.5 ml saline, and 20 μl solution was taken out and inoculated on MRS solid medium to observe colony growth. The same testing method was used to assess the viability of *L. reuteri* in 5 % GL MN patches under the storage condition at 4 °C. Furthermore, to evaluate the survival of *L. reuteri* in vivo, the fur on the backs of the mice was shaved, and *L. reuteri* (10^8 CFU) was transdermally delivered using a 5 % GL MN patch. The probiotic of *L. reuteri* was extracted from the skin site, and dispersed in 20 μl saline on days 0, 3, 5, 7 and 9. Finally, the solution was inoculated onto MRS solid medium to observe colony growth.

4.19. Wound healing test of 5 % GL MN patches

All animal experiments were performed according to the protocols approved by the Institutional Animal Care and Use Committee of Wuhan University (WP20230362). SPF BALB/c female mice (18–20 g) with approval number SCXK 2020–0005 were used to evaluate the wound-healing capability of the MN patches in vivo. After a week of adaptation, the mice were randomly divided into five groups (n = 7). Each mouse was anesthetized with 0.05 ml of 20 mg/ml pentobarbital sodium, and a round wound with a diameter of 1 cm was created on the back of the mouse. Subsequently, 100 μl *S. aureus* suspension (10^8 CFU/ml) was inoculated on the wound surface to establish a wound infection model. The mice received different treatments 2 days post-inoculation: 1) no treatment (Control), 2) MN patch loaded with reuterin (RE MNs), 3) MN patch made of PVA-sucrose matrix alone (PVA-S MNs), 4) MN patch loaded with *L. reuteri* without glycerol (0 % GL MNs), and 5) MN patch loaded with *L. reuteri* and 5 % glycerol (5 % GL MNs), with the application time of 4 min for each MN patch in vivo. Images of the wounds in each group were captured on days 0, 3, 5, 7, and 9 after treatment. *S. aureus* was isolated from the wounds and cultured on LB solid medium to observe bacterial growth and evaluate the antibacterial effect in each group. Additionally, the body weights of mice were measured during wound healing. The formula for calculating the wound-remaining ratio is:

$$Wound\ remaining\ ratio\ (\%) = \frac{Actual\ wound\ area}{Original\ wound\ area} \times 100\%.$$

4.20. Histological analysis

After 9 days of application of the MN patches, the mice were euthanized, and skin around the back wounds were cut off, followed by fixation in a 4 % paraformaldehyde solution for 24 h. Then, the samples were embedded in paraffin and cut into 5 μm-thick tissue sections for histological analysis. ImageJ software was used to calculate the epidermal thickness, collagen volume fraction, IL-6 positivity rate, and neovascularization coverage of the wound. The major organs of each group, including the heart, liver, spleen, lungs, and kidneys, were collected for H&E staining.

4.21. Statistical analysis

All the results presented in this study are means ± standard deviation (SD). Statistical analysis was performed using a two-sided Student's t-test or one-way analysis of variance (ANOVA) in Excel. $P < 0.05$ was considered significant. The levels of significance were labeled as *$P < 0.05$, **$P < 0.01$, and ***$P < 0.001$.

Ethics approval and consent to participate

All the animal studies were following the guidelines of the Institutional Animal Care and Use Committee (IACUC) of Wuhan University, and were approved by the animal ethics committee of Wuhan University (reference number: WP20230362).

Data availability statement

Data supporting the findings of this study are available from the corresponding author upon request.

CRediT authorship contribution statement

Yinli Jin: Writing – original draft, Software, Methodology, Formal analysis, Data curation, Conceptualization. **Yun Lu:** Supervision, Methodology. **Xue Jiang:** Software, Project administration, Methodology. **Min Wang:** Methodology, Formal analysis, Data curation. **Yaqi Yuan:** Validation, Supervision. **Yongnian Zeng:** Methodology, Funding acquisition. **Liang Guo:** Writing – review & editing, Visualization, Validation, Supervision, Funding acquisition, Formal analysis. **Wei Li:** Writing – review & editing, Supervision, Methodology, Funding acquisition.

Declaration of competing interest

The authors declare that they have no competing interests.

Appendix A. Supplementary data

Supplementary data to this article can be found online at https://doi.org/10.1016/j.bioactmat.2024.05.008.

References

[1] A.C. Johnson, E.P. Buchanan, D.Y. Khechoyan, Wound infection: a review of qualitative and quantitative assessment modalities, J. Plast. Reconstr. Aesthetic Surg. 75 (4) (2022) 1287–1296.
[2] E.F. Ahmed, A.H. Rasmi, A.M.A. Darwish, G.F.M. Gad, Prevalence and resistance profile of bacteria isolated from wound infections among a group of patients in upper Egypt: a descriptive cross-sectional study, BMC Res. Notes 16 (1) (2023) 106.
[3] M. Falcone, B. De Angelis, F. Pea, A. Scalise, S. Stefani, R. Tasinato, et al., Challenges in the management of chronic wound infections, J Glob Antimicrob Resist 26 (2021) 140–147.
[4] J.S. Mervis, T.J. Phillips, Pressure ulcers: Prevention and management, J. Am. Acad. Dermatol. 81 (4) (2019) 893–902.
[5] C. Tu, H. Lu, T. Zhou, W. Zhang, L. Deng, W. Cao, et al., Promoting the healing of infected diabetic wound by an anti-bacterial and nano-enzyme-containing hydrogel with inflammation-suppressing, ROS-scavenging, oxygen and nitric oxide-generating properties, Biomaterials 286 (2022) 121597.
[6] H. Zhou, Q. Jin, H. Lu, Exposure risk of patients with chronic infectious wounds during the COVID-19 outbreak and its countermeasures, J. Orthop. Surg. Res. 15 (1) (2020) 452.
[7] A. Pormohammad, N.K. Monych, S. Ghosh, D.L. Turner, R.J. Turner, Nanomaterials in wound healing and infection control, Antibiotics (Basel) 10 (5) (2021) 473.
[8] B.A. Lipsky, A.R. Berendt, P.B. Cornia, J.C. Pile, E.J. Peters, D.G. Armstrong, et al., Infectious Diseases Society of America clinical practice guideline for the diagnosis and treatment of diabetic foot infections, Clin. Infect. Dis. 54 (12) (2012) e132–e173, 2012.
[9] W.S. Joseph, M.A. Kosinski, L.C. Rogers, Parenteral Vancomycin in the treatment of MRSA-associated diabetic foot infections: an Unnecessary risk, Int. J. Low. Extrem. Wounds (2023) 15347346231207553.

[10] K. Huang, W. Liu, W. Wei, Y. Zhao, P. Zhuang, X. Wang, et al., Photothermal hydrogel encapsulating Intelligently bacteria-capturing bio-MOF for infectious wound healing, ACS Nano 16 (11) (2022) 19491–19508.

[11] P.A. Shiekh, A. Singh, A. Kumar, Exosome laden oxygen releasing antioxidant and antibacterial cryogel wound dressing OxOBand alleviate diabetic and infectious wound healing, Biomaterials 249 (2020) 120020.

[12] Z. Liu, J.C. Dumville, R.J. Hinchliffe, N. Cullum, F. Game, N. Stubbs, et al., Negative pressure wound therapy for treating foot wounds in people with diabetes mellitus, Cochrane Database Syst. Rev. 10 (10) (2018) Cd010318.

[13] X. Liu, H. Zhang, S. Cen, F. Huang, Negative pressure wound therapy versus conventional wound dressings in treatment of open fractures: a systematic review and meta-analysis, Int. J. Surg. 53 (2018) 72–79.

[14] Y. Hao, W. Zhao, H. Zhang, W. Zheng, Q. Zhou, Carboxymethyl chitosan-based hydrogels containing fibroblast growth factors for triggering diabetic wound healing, Carbohydr. Polym. 287 (2022) 119336.

[15] P. Wu, X. Liu, Y. Duan, L. Pan, Z. Sun, H. Chu, et al., ZnPc photosensitizer-loaded peony-shaped FeSe2 remotely controlled by near-infrared light for antimycobacterial therapy, Acta Materia Medica 2 (2) (2023) 260–269.

[16] C. Cao, T. Zhang, N. Yang, X. Niu, Z. Zhou, J. Wang, et al., POD Nanozyme optimized by charge separation engineering for light/pH activated bacteria catalytic/photodynamic therapy, Signal Transduct Target Ther 7 (1) (2022) 86.

[17] Y. Qiao, Y. Ping, H. Zhang, B. Zhou, F. Liu, Y. Yu, et al., Laser-activatable CuS nanodots to treat multidrug-resistant bacteria and release copper ion to accelerate healing of infected chronic nonhealing wounds, ACS Appl. Mater. Interfaces 11 (4) (2019) 3809–3822.

[18] R. Roy, M. Tiwari, G. Donelli, V. Tiwari, Strategies for combating bacterial biofilms: a focus on anti-biofilm agents and their mechanisms of action, Virulence 9 (1) (2018) 522–554.

[19] S. Gopalakrishnan, A. Gupta, J.M.V. Makabenta, J. Park, J.J. Amante, A. N. Chattopadhyay, et al., Ultrasound-enhanced antibacterial activity of polymeric nanoparticles for eradicating bacterial biofilms, Adv Healthc Mater 11 (21) (2022) e2201060.

[20] F. Zhao, Y. Su, J. Wang, S. Romanova, D.J. DiMaio, J. Xie, et al., A highly efficacious electrical biofilm treatment system for combating chronic wound bacterial infections, Adv Mater 35 (6) (2023) e2208069.

[21] C. Llor, L. Bjerrum, Antimicrobial resistance: risk associated with antibiotic overuse and initiatives to reduce the problem, Ther Adv Drug Saf 5 (6) (2014) 229–241.

[22] L. Teot, N. Ohura, Challenges and management in wound Care, Plast. Reconstr. Surg. 147 (1s-1) (2021) 9s–15s.

[23] Q. Tang, N. Xue, X. Ding, K.H. Tsai, J.J. Hew, R. Jiang, et al., Role of wound microbiome, strategies of microbiota delivery system and clinical management, Adv. Drug Deliv. Rev. 192 (2023) 114671.

[24] Q. Mu, V.J. Tavella, X.M. Luo, Role of Lactobacillus reuteri in human health and diseases, Front. Microbiol. 9 (2018) 757.

[25] M.A. Engevik, W. Ruan, M. Esparza, R. Fultz, Z. Shi, K.A. Engevik, et al., Immunomodulation of dendritic cells by Lactobacillus reuteri surface components and metabolites, Physiol Rep 9 (2) (2021) e14719.

[26] Z. Ming, L. Han, M. Bao, H. Zhu, S. Qiang, S. Xue, et al., Living bacterial hydrogels for accelerated infected wound healing, Adv. Sci. 8 (24) (2021) e2102545.

[27] L. Mei, D. Zhang, H. Shao, Y. Hao, T. Zhang, W. Zheng, et al., Injectable and self-healing probiotics-loaded hydrogel for promoting superbacteria-infected wound healing, ACS Appl. Mater. Interfaces 14 (18) (2022) 20538–20550.

[28] Y. Xiao, C. Lu, Y. Liu, L. Kong, H. Bai, H. Mu, et al., Encapsulation of Lactobacillus rhamnosus in hyaluronic acid-based hydrogel for pathogen-targeted delivery to ameliorate enteritis, ACS Appl. Mater. Interfaces 12 (33) (2020) 36967–36977.

[29] C. Gonzalez-Ferrero, J.M. Irache, C.J. Gonzalez-Navarro, Soybean protein-based microparticles for oral delivery of probiotics with improved stability during storage and gut resistance, Food Chem. 239 (2018) 879–888.

[30] J. Xie, M. Yao, Y. Lu, M. Yu, S. Han, D.J. McClements, et al., Impact of encapsulating a probiotic (Pediococcus pentosaceus Li05) within gastro-responsive microgels on Clostridium difficile infections, Food Funct. 12 (7) (2021) 3180–3190.

[31] C. Li, Z.X. Wang, H. Xiao, F.G. Wu, Intestinal delivery of probiotics: materials, strategies, and applications, Adv Mater (2024) e2310174.

[32] K. Cheung, D.B. Das, Microneedles for drug delivery: trends and progress, Drug Deliv. 23 (7) (2016) 2338–2354.

[33] M. Avcil, A. Celik, Microneedles in drug delivery: progress and challenges, Micromachines 12 (11) (2021).

[34] T. Liu, M. Chen, J. Fu, Y. Sun, C. Lu, G. Quan, et al., Recent advances in microneedles-mediated transdermal delivery of protein and peptide drugs, Acta Pharm. Sin. B 11 (8) (2021) 2326–2343.

[35] W. Li, R.N. Terry, J. Tang, M.R. Feng, S.P. Schwendeman, M.R. Prausnitz, Rapidly separable microneedle patch for the sustained release of a contraceptive, Nat. Biomed. Eng. 3 (3) (2019) 220–229.

[36] J. Yu, Y. Zhang, Y. Ye, R. DiSanto, W. Sun, D. Ranson, et al., Microneedle-array patches loaded with hypoxia-sensitive vesicles provide fast glucose-responsive insulin delivery, Proc Natl Acad Sci U S A 112 (27) (2015) 8260–8265.

[37] Y. Zhou, L. Jia, D. Zhou, G. Chen, Q. Fu, N. Li, Advances in microneedles research based on promoting hair regrowth, J Control Release 353 (2023) 965–974.

[38] Y. Yang, Z. Li, P. Huang, J. Lin, J. Li, K. Shi, et al., Dissolving microneedles with sustained-release colchicine and stabilized uricase for simplified long-term gout management, Acta Pharm. Sin. B 13 (8) (2023) 3454–3470.

[39] A.F. Moreira, C.F. Rodrigues, T.A. Jacinto, S.P. Miguel, E.C. Costa, I.J. Correia, Microneedle-based delivery devices for cancer therapy: a review, Pharmacol. Res. 148 (2019) 104438.

[40] B. Cai, Y. Gong, Z. Wang, L. Wang, W. Chen, Microneedle arrays integrated with living organisms for smart biomedical applications, Theranostics 11 (20) (2021) 10012–10029.

[41] H.J. Chen, D.A. Lin, F. Liu, L. Zhou, D. Liu, Z. Lin, et al., Transdermal delivery of living and biofunctional probiotics through dissolvable microneedle patches, ACS Appl. Bio Mater. 1 (2) (2018) 374–381.

[42] C.K. Enggi, S. Sulistiawati, S. Stephanie, F. Tangdilintin, A.A. Achmad, R.A. Putri, et al., Development of probiotic loaded multilayer microcapsules incorporated into dissolving microneedles for potential improvement treatment of vulvovaginal candidiasis: a proof of concept study, J. Colloid Interface Sci. 648 (2023) 203–219.

[43] S.A. Lopes, C.A. Roque-Borda, J.L. Duarte, L.D. Di Filippo, V.M.B. Cardoso, F. R. Pavan, et al., Delivery strategies of probiotics from nano- and microparticles: trends in the treatment of inflammatory bowel disease-an overview, Pharmaceutics 15 (11) (2023).

[44] Y.H. Sun, M.X. Liu, X.D. Tang, Y.M. Zhou, J.H. Zhang, B. Yang, Culture-delivery live probiotics dressing for accelerated infected wound healing, Acs Applied Materials & Interfaces 15 (46) (2023) 53283–53296.

[45] K. Huang, W. Shi, B. Yang, J. Wang, The probiotic and immunomodulation effects of Limosilactobacillus reuteri RGW1 isolated from calf feces, Front. Cell. Infect. Microbiol. 12 (2022) 1086861.

[46] J.A. Linares-Pastén, R. Sabet-Azad, L. Pessina, R.R. Sardari, M.H. Ibrahim, R. Hatti-Kaul, Efficient poly(3-hydroxypropionate) production from glycerol using Lactobacillus reuteri and recombinant Escherichia coli harboring L. reuteri propionaldehyde dehydrogenase and Chromobacterium sp. PHA synthase genes, Bioresour. Technol. 180 (2015) 172–176.

[47] R. De Weirdt, A. Crabbé, S. Roos, S. Vollenweider, C. Lacroix, J.P. van Pijkeren, et al., Glycerol supplementation enhances L. reuteri's protective effect against S. Typhimurium colonization in a 3-D model of colonic epithelium, PLoS One 7 (5) (2012) e37116.

[48] V. Cleusix, C. Lacroix, S. Vollenweider, M. Duboux, G. Le Blay, Inhibitory activity spectrum of reuterin produced by Lactobacillus reuteri against intestinal bacteria, BMC Microbiol. 7 (2007) 101.

[49] L. Schaefer, T.A. Auchtung, K.E. Hermans, D. Whitehead, B. Borhan, R.A. Britton, The antimicrobial compound reuterin (3-hydroxypropionaldehyde) induces oxidative stress via interaction with thiol groups, Microbiology (Read.) 156 (Pt 6) (2010) 1589–1599.

[50] A. Banu, M.M. Noorul Hassan, J. Rajkumar, S. Srinivasa, Spectrum of bacteria associated with diabetic foot ulcer and biofilm formation: a prospective study, Australas. Med. J. 8 (9) (2015) 280–285.

[51] F. Sadeghpour Heravi, M. Zakrzewski, K. Vickery, G.A. D, H. Hu, Bacterial diversity of diabetic foot ulcers: current status and future prospectives, J. Clin. Med. 8 (11) (2019).

[52] V.A. Baldassarro, L. Lorenzini, A. Giuliani, M. Cescatti, G. Alastra, M. Pannella, et al., Molecular mechanisms of skin wound healing in non-diabetic and diabetic mice in excision and pressure experimental wounds, Cell Tissue Res. 388 (3) (2022) 595–613.

[53] A. Grada, J. Mervis, V. Falanga, Research techniques made simple: animal models of wound healing, J. Invest. Dermatol. 138 (10) (2018) 2095–2105 e2091.

[54] W. Ma, X. Zhang, Y. Liu, L. Fan, J. Gan, W. Liu, et al., Polydopamine decorated microneedles with Fe-MSC-Derived nanovesicles encapsulation for wound healing, Adv. Sci. 9 (13) (2022) e2103317.

[55] G. Zheng, J. Xie, Y. Yao, S. Shen, J. Weng, Q. Yang, et al., MgO@polydopamine nanoparticle-loaded photothermal microneedle patches combined with chitosan gel dressings for the treatment of infectious wounds, ACS Appl. Mater. Interfaces 16 (10) (2024) 12202–12216.

[56] Z.Q. Zhao, L. Liang, L.Y. Jing, Y. Liu, Y.H. Zhang, M.A. Shahbazi, et al., Microneedles: a novel strategy for wound management, Biomater. Sci. 11 (13) (2023) 4430–4451.

[57] L. Long, W. Liu, C. Hu, L. Yang, Y. Wang, Construction of multifunctional wound dressings with their application in chronic wound treatment, Biomater. Sci. 10 (15) (2022) 4058–4076.